Nanoscale Advances

ROYAL SOCIETY OF CHEMISTRY

PAPER

View Article Online
View Journal | View Issue

Cite this: *Nanoscale Adv.*, 2024, **6**, 3158

RSM optimization of Friedel–Crafts *C*-acylation of *para*-fluorophenol over the catalysis of phosphomolybdic acid encapsulated in MIL-53 (Fe) metal organic frameworks

Ahmad Nikseresht, *[a] Reza Mehravar[a] and Masoud Mohammadi [b]

Received 17th December 2023
Accepted 10th April 2024

DOI: 10.1039/d3na01126g

rsc.li/nanoscale-advances

In this research, a heterogeneous acid catalyst was synthesized by room temperature encapsulation of phosphomolybdic acid (PMA) in the pores of the MIL-53 (Fe) metal organic framework (MOF) under ultrasonic conditions. Then the catalytic activity of PMA@MIL-53 (Fe) was investigated in Friedel–Crafts *C*-acylation of *para*-fluorophenol, and this procedure was optimized using response surface methodology based on central composite design (RSM-CCD). The impact of critical reaction parameters including reaction duration, catalyst dosage, and PMA amount in the catalyst was optimized, leading to the formation of the target product in excellent yield at a short reaction time.

1. Introduction

The Friedel–Crafts reactions are widely used in organic synthesis for the introduction of new substituents onto aromatic rings.[1] Among these reactions, Friedel–Crafts alkylation and acylation are two of the most commonly employed methods.[2] While both reactions have their own merits and limitations, the choice of reaction largely depends on the nature of the substituent to be introduced.[2] In recent years, Friedel–Crafts acylation has gained increasing attention as a suitable alternative to Friedel–Crafts alkylation in mono-substitution of aromatic rings.[3] This is due to the fact that Friedel–Crafts acylation offers several advantages over Friedel–Crafts alkylation, including higher selectivity, milder reaction conditions, and fewer side reactions.[4] This acylation method involves the electrophilic substitution of an aromatic ring with an acyl group. This reaction has been extensively studied since its discovery in the late 19th century and has become a key tool for the preparation of a wide range of organic compounds, including in the fields of pharmaceuticals, agrochemicals, and materials science.[5] The success of this reaction relies on the use of Lewis acid catalysts, such as aluminum chloride, and a variety of acylating agents, including acid chlorides, anhydrides, and esters.[4] Despite its broad applicability, the Friedel–Crafts acylation mechanism is still subject to debate, with various proposals for the formation of the key intermediates and transition states. Based on the recent experimental and computational studies that shed light on the reaction mechanism, this process probably is thought to involve the creation of a complex between a Lewis acid and a chlorine atom from the acid chloride, which then leads to the formation of an acylium ion through the breaking of the C–Cl bond. This reactive intermediate has a positively charged carbon and is stabilized through resonance, which acts as an electrophile and reacts with the arene to produce the mono-acylated product through formation of a new carbon–carbon bond, which is an aryl ketone.[6–8]

Aluminum chloride is a popular catalyst in aromatic substitution reactions due to its effectiveness. However, it has some drawbacks, such as instability and temperature sensitivity. Additionally, aluminum chloride can ignite combustibles and react with water and wet air to produce hazardous hydrogen chloride gas and heat. Furthermore, this Lewis acid can cause equipment deterioration and generate a significant amount of waste during the deactivation of the catalytic complex.[4] In recent times, a variety of catalysts have been employed in this reaction. The entire process generates a significant amount of hazardous waste that is challenging to separate from the target product.[9,10] Solid acid catalysts that are recyclable and environment-friendly, such as metal–organic frameworks (MOFs), are preferred because of their advantages. This will decrease the impact of environmental and economic issues.

Metal–organic frameworks (MOFs), a series of porous materials with adjustable chemical and physical characteristics, are one of the most widely used materials for the heterogenization of solid acids.[11–16] These materials' adaptable structure enables a wide range of chemical processes, such as catalysis, photocatalysis, electrocatalysis, adsorption, separation, sensing, drug administration, and organic transformation.[16–20] The acidity of MOFs can be tuned by changing the metal node or ligand's functional group, allowing for the selective activation of specific functional groups in the reactants.[21] In particular, supported phosphomolybdic acid catalysts

[a]*Department of Chemistry, Payame Noor University, PO BOX 19395-4697, Tehran, Iran*
[b]*Department of Chemistry, Faculty of Science, Ilam University, P.O. Box 69315516, Ilam, Iran. E-mail: a_nik55@yahoo.com; ahmad.nikseresht@pnu.ac.ir; Tel: +98-918-8418754*

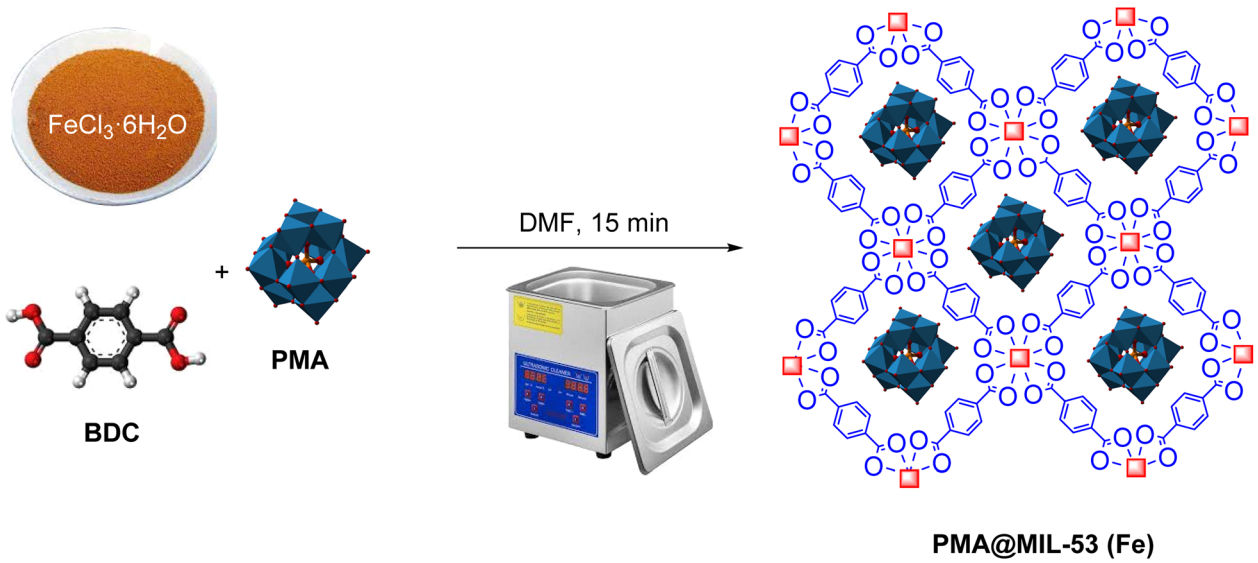

Scheme 1 Synthesis of PMA@MIL-53 (Fe) MOF (schematic structure).

have been used in various organic reactions, including esterification, transesterification, aldol condensation, Friedel–Crafts acylation, *etc.*[22–28] We have just recently achieved the synthesis of a phosphomolybdic acid-based catalyst that is prepared by encapsulation of phosphomolybdic acid groups in the MIL-53 (Fe) MOF pores by employing a simple one-pot approach.[11] This acid was characterized as having a high level of thermal stability, a large surface area, efficient catalytic activity, and reusability.[11] Herein, we demonstrate the catalytic application of this solid acid catalyst for selective Friedel–Crafts *C*-acylation of *para*-fluorophenol utilizing acetyl chloride as an effective acylating agent.

2. Experimental

2.1. Materials

The Merck Millipore company supplied all of the components and solvents, which were then put to use without undergoing any additional purification steps.

2.2. General procedure for the encapsulation of phosphotungstic acid in MIL-53 (Fe) (PTA@MIL-53 (Fe))

According to the findings that were obtained from our previous report,[11] PMA@MIL-53 (Fe) was synthesized *via* employing a one-pot ultrasonic assisted procedure. In this sense, the standard process involves dissolving 1 mmol of $FeCl_3 \cdot 6H_2O$, 1 mmol of 1,4-benzendicarboxylic acid (1,4-BDC) and varying quantities of phosphomolybdic acid hydrate (PMA) (0.01 and 0.02 g) in 5 mL of dimethylformamide (DMF). Afterwards, the mixture was placed in an ultrasonic bath for 15 minutes at a frequency of 37 kHz and an output power of 240 W. The temperature of the bath was kept at room temperature throughout the process. Following that, the product was filtered with a Büchner funnel, the obtained powder was washed using DMF under Vacuum filtration and, then, it was dried in a vacuum at a temperature of 150 °C for 15 h (Scheme 1).

2.3. General procedure for the Friedel–Crafts *C*-acylation of *para*-fluorophenol over the catalysis of PMA@MIL-53 (Fe) MOF

A mixture of 4-fluorophenol (7 mmol), acetyl chloride (7 mmol), and 30–200 mg of PMA@MIL-53 (Fe) as the catalyst comprising various levels of PMA (5–30%) was put into a 25 mL round bottom flask and, then, it was stirred at room temperature for 10–50 minutes. After a specified time period based on the test parameters, the catalyst was collected by centrifugation from the diluted mixture. It was then extracted with ethyl acetate, washed, and dried, and the solvent was evaporated. Finally, the crude products were purified using a silica gel plate (Scheme 2).

3. Results and discussion

3.1. Characterization

The as-prepared phosphomolybdic acid encapsulated within the MIL-53 (Fe) MOF was previously subjected to thorough

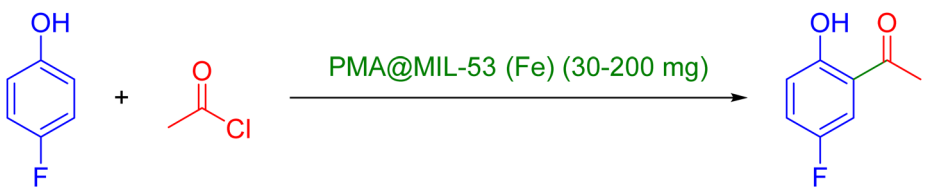

Scheme 2 Friedel–Crafts *C*-acylation of *para*-fluorophenol over the catalysis of PMA@MIL-53 (Fe) MOF.

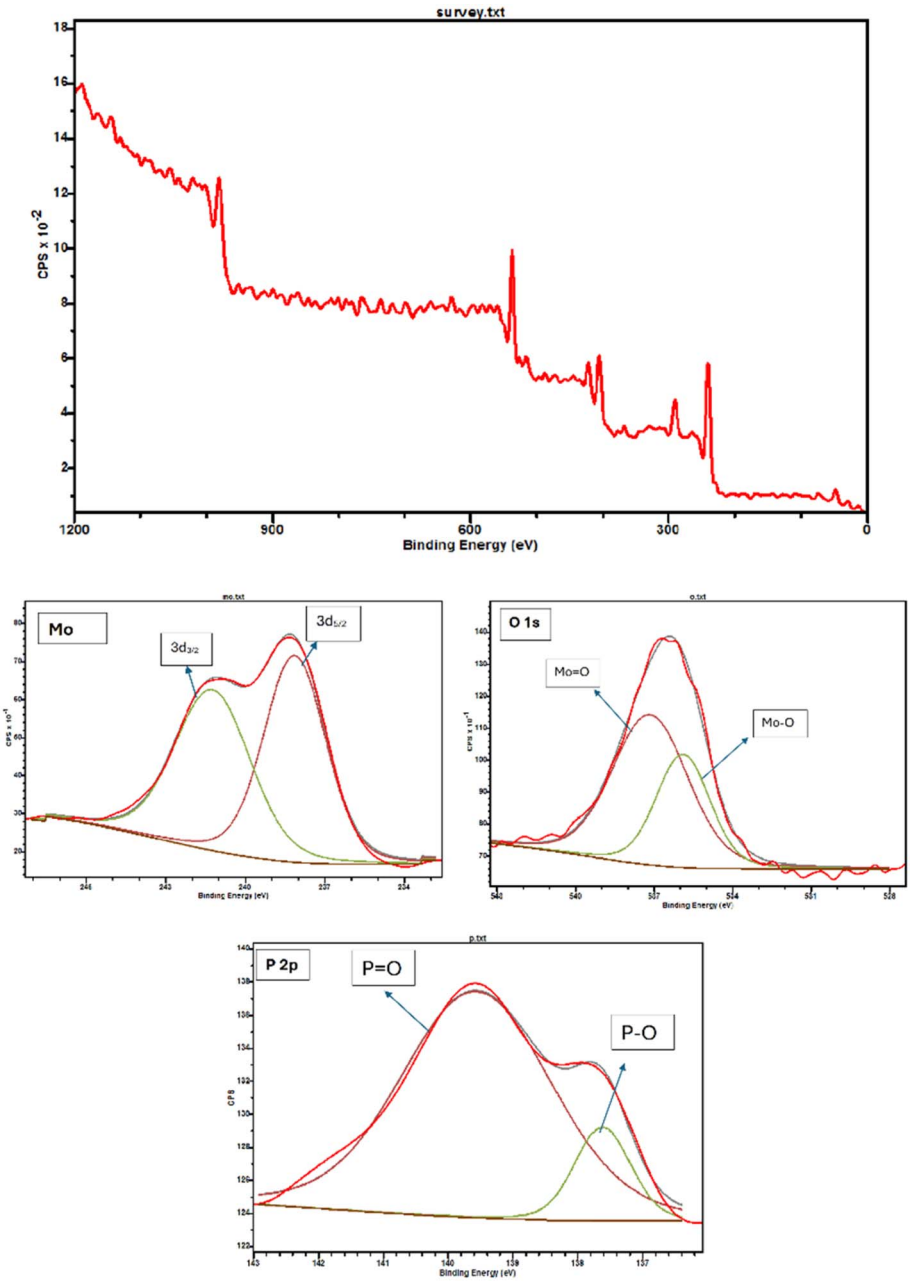

Fig. 1 XPS analysis of phosphomolybdic acid.

characterization in our laboratory. This involved employing a range of analytical techniques such as Fourier-transform infrared spectroscopy (FT-IR), X-ray diffraction (XRD), X-ray photoelectron spectroscopy (XPS), thermogravimetric analysis (TGA), energy-dispersive X-ray spectroscopy (EDS), inductively coupled plasma optical emission spectrometry (ICP-OES), X-ray mapping, field emission scanning electron microscopy (FE-SEM), high-resolution transmission electron microscopy (HR-TEM), and nitrogen adsorption–desorption analysis.[11] In this report, our primary aim was to provide a more comprehensive characterization of the PMA@MIL-53 (Fe) MOF. To achieve this, we ensured thorough completion of catalyst characterization, including XPS analysis of pure phosphomolybdic acid for the purpose of comparison.

The XPS analysis depicted in Fig. 1 illustrates the elemental composition and chemical bonding of phosphomolybdic acid (PMA). Consisting primarily of phosphorus, molybdenum, and oxygen, this compound reveals distinctive peaks corresponding to its constituent elements and their bonding configurations. In the spectrum, the characteristic peaks for the P–O and P═O bonds within PMA emerge prominently at 137.6 and 139.5 eV, respectively. Molybdenum, predominantly existing in the +6 oxidation state, exhibits discernible signals for Mo: $3d_{3/2}$ and Mo: $3d_{5/2}$ at 241.1 and 238.1 eV, respectively. Likewise, the Mo–O and Mo═O bonds manifest distinct peaks at 537.1 eV and 535.8 eV, elucidating the chemical environment surrounding molybdenum within the compound. These findings align closely with

Table 1 The experimental results of Fries rearrangement reaction design expert analysis

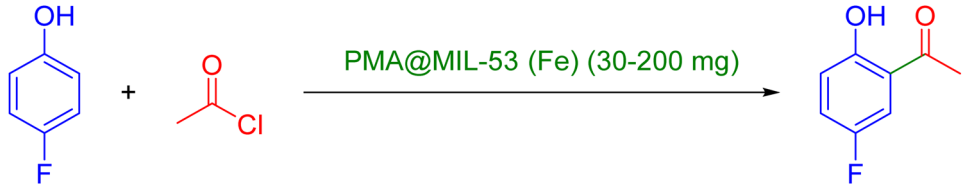

	Independent variables			Response
Run	Time (min)	Catalyst loading (mg)	PMA (wt%)	Yield[a] (%)
1	18	165.54	24.93	59
2	42	164.46	24.93	67
3	30	115	17.50	79
4	10	115	17.50	26
5	30	200	17.50	73.1
6	30	115	5.00	15
7	30	115	17.50	81.8
8	18	64.46	24.93	15.5
9	18	165.54	10.07	29
10	42	165.54	10.07	18
11	42	64.46	10.07	34
12	42	165.54	24.93	96.3
13	18	64.46	10.07	9
14	50	115	17.50	81.8
15	30	115	30.00	81
16	30	30	17.50	29
17	30	115	17.50	76

[a] Isolated yield.

our prior investigations on PMA@MIL-53 (Fe) MOF by XPS analysis[11] and provide conclusive evidence regarding the presence of phosphomolybdic acid within the catalyst structure. The agreement between these results and previous reports underscores the reliability of our analytical methodology and reinforces our understanding of PMA's role in catalytic processes.

3.2. Design expert

The CCD method is more effective than other RSM methods because it covers a larger operability region and accurately predicts the center point, regardless of missing data points. Thus, Friedel–Crafts *C*-acylation of *para*-fluorophenol using the PMA@MIL-53 (Fe) MOF catalyst was designed with the CCD technique, focusing on reaction time, catalyst amount, and PMA weight percent as key parameters affecting *para*-fluorophenol conversion and acylated product yield. The experiment was conducted at room temperature in line with green chemistry principles, and five-level coded factors (, 1, 0, +1, +) were considered with corresponding values presented in Table 1. The parameter ranges for the initial experiment design were selected based on preliminary tests.

3.3. Effects of reaction parameters on the *C*-acylated yield

The following plots were made in order to demonstrate the impacts of two factors having an influence on the response while the third variable remains unchanged.

3.3.1 Effect of reaction time and PMA percentage parameters. The interaction between the percentage of PMA loaded and the response time is shown in Fig. 2. From this plot, it can be concluded that increasing the reaction time leads to an increase in the *C*-acylation yield. In other words, increasing the response time through increasing the amount of effective and efficient encounters and increasing the penetration coefficient increases the yield of the corresponding product. By increasing the percentage of PMA, more active sites of the catalyst particles are provided, and by increasing the number of molecules of raw materials involved in the reaction with appropriate activation energy, the speed of the reaction also increases and the amount of *C*-acylation of the product increases dramatically. Also, when the reaction time is considered constant, with an increase in the percentage of PMA, the amount of the product also increases greatly. This phenomenon can be related to the increase in the ability of heteropoly acids to produce stable surface-active sites, which leads to the unique distribution of the active phase and the creation of numerous active sites to carry out reactions and increase efficiency.

3.3.2 Mutual effect of reaction time and the catalyst amount parameters. The interaction between the catalyst amount and reaction time parameters is presented in Fig. 3. It

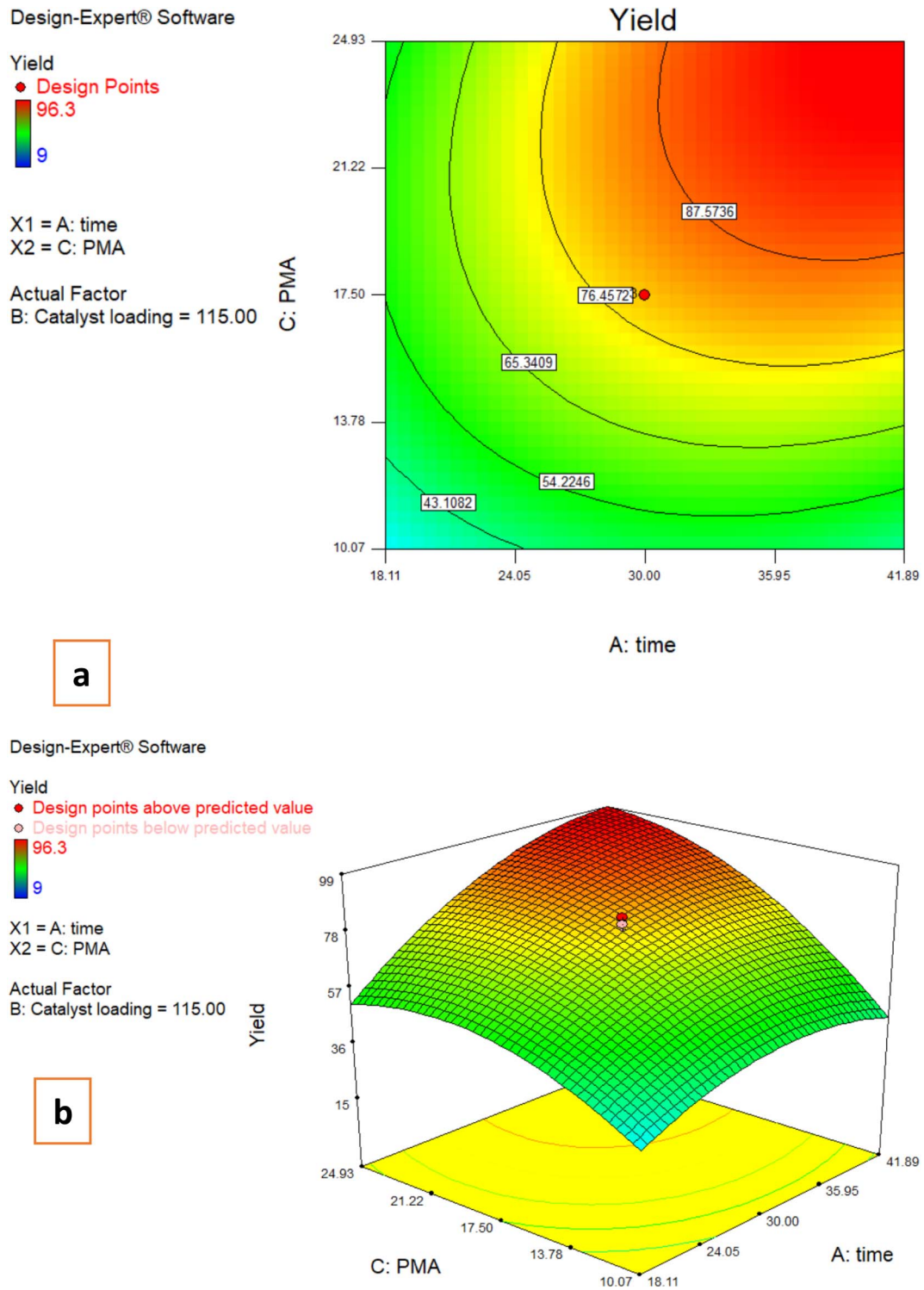

Fig. 2 (a) Contour and (b) three-dimensional diagrams showing the interaction effect of two processes, reaction time and PMA percentage on the production process of the *C*-acylation product.

can be seen that when the reaction time remains constant, with an increase in the amount of the catalyst, the amount of the *C*-acylation product increases. Because when the amount of loaded catalyst increases, the active sites of the reactant also increase, which leads to an increase in effective interactions in the reaction, and an increase in the reaction speed.

3.3.3 Mutual effect of the catalyst amount and the PMA percentage parameters. Friedel–Crafts acylation reaction of *para*-fluorophenol with acyl chloride using the 53MIL@PMA MOF (Fe) catalyst has been carried out for all the entries in Table 1, and the optimization results are as follows. Fig. 4 shows the interaction between the amount of catalyst and the percentage of PMA and

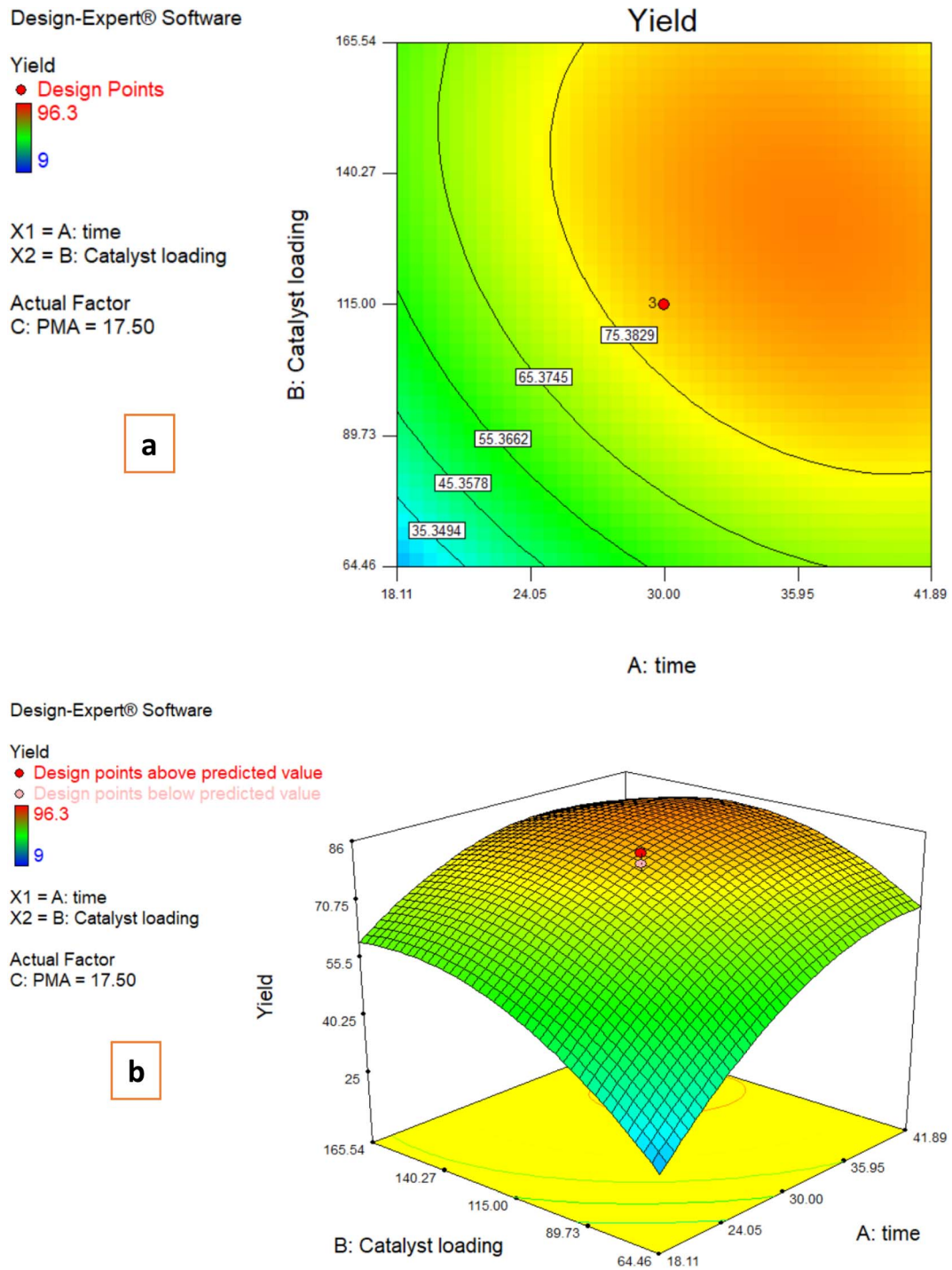

Fig. 3 (a) Contour and (b) three-dimensional diagrams showing the mutual effect of reaction time and catalyst amount on the efficiency of the production process of the *C*-acylation product.

their mutual effects on the formation of the *C*-acylation (*ortho*) product of *para*-fluorophenol production. It can be clearly seen that when the amount of catalyst is at its high values and the percentage of PMA is at its maximum values, the efficiency of the system is maximum. It is obvious that with the increase of the catalyst, the efficiency also increases because with the other parameters remaining constant and the increase in the amount of the catalyst, the number of active sites for the reaction will also increase, which will increase the speed of the Friedel–Crafts acylation yield. Also, the increase in the amount of PMA up to 60% also improves the production process because the increase in the amount of PMA causes the unique spread of the active phase and the creation of countless active sites to perform reactions, resulting in a significant improvement in activity, selectivity, efficiency and stability.

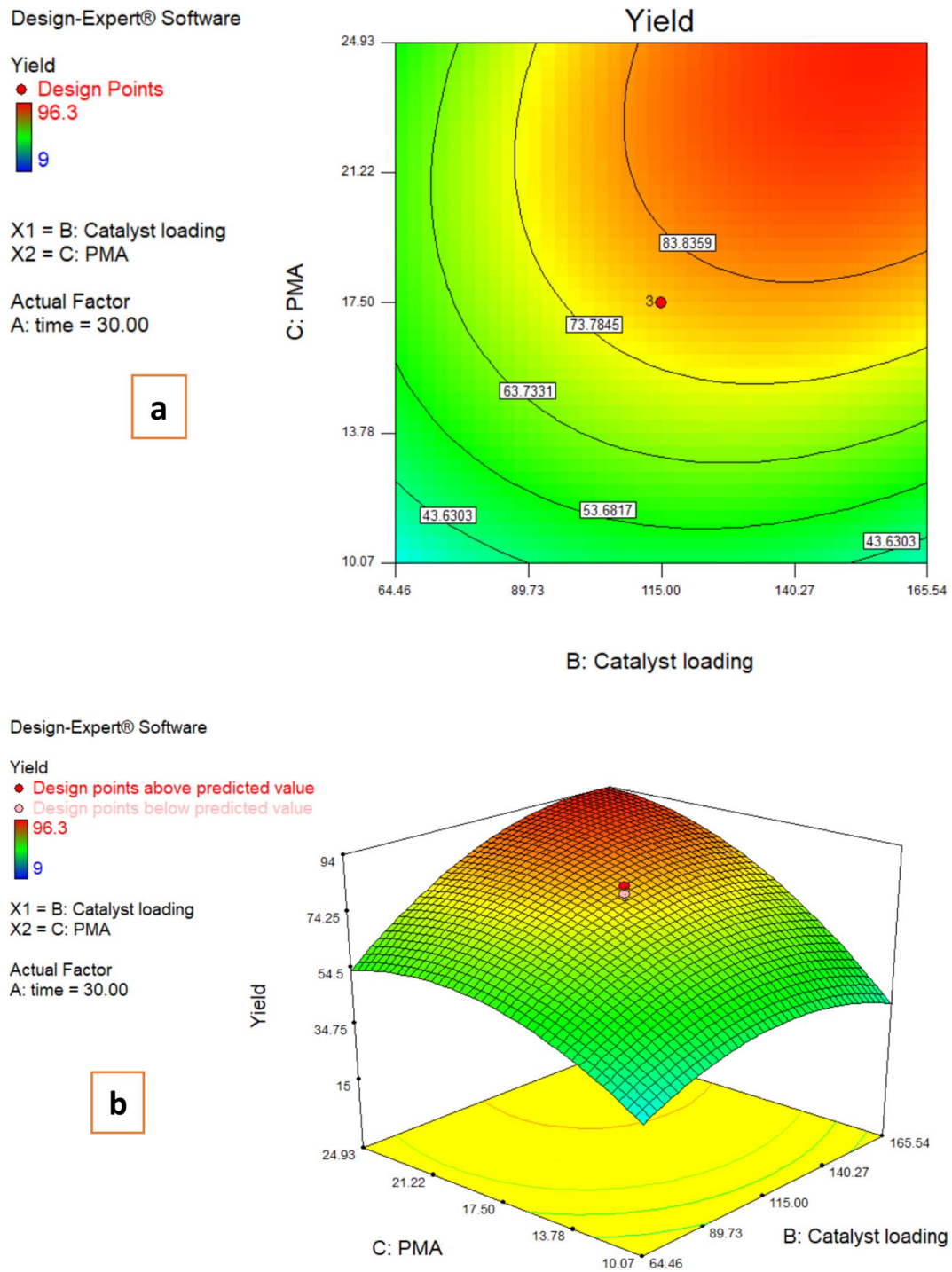

Fig. 4 (a) Contour and (b) three-dimensional diagrams showing the mutual effect of reaction time and catalyst amount on the efficiency of the production process of the *C*-acylation product.

3.4. Model development

The RSM was applied to create a mathematical model and analyze how the variables and their interactions affected the response. Additionally, a trivariate CCD was employed to determine the impact of different factors on the amount of *C*-acylated produced. To predict the yield, an equation was suggested.

$$\text{Yield (\%) in Fries rearrangement reaction} = 79.47 + 14.40 \times \text{time} + 11.05 \times \text{catalyst loading} + 18.95 \times \text{PMA} - 6.28\text{time} \times \text{catalyst loading} + 9.35\text{time} \times \text{PMA} + 8.60B \times \text{PMA} - 10.70 \times \text{time}^2 - 11.70 \times \text{catalyst loading}^2 - 12.78 \times \text{PMA}^2$$

3.4.1 ANOVA analysis. The obtained results were analyzed using the analysis of variance method (ANOVA) using the

Table 2 ANOVA for the regression model and respective model terms for the product yield of Friedel–Crafts *C*-acylation of *para*-fluorophenol

Source	Sum of squares	Df[a]	Mean square	*F*-Value[b]	*p*-Value (prob > *F*) [c]	
Model	13 969.26	9	1525.14	28.00	0.0001	Significant
A-Reaction time	2831.46	1	2831.46	51.08	0.0002	
B-Catalyst loading	1668.84	1	1668.84	30.10	0.0009	
C-PMA	4904.25	1	4904.25	88.47	<0.0001	
AB	315.01	1	315.01	5.68	0.0486	
AC	699.38	1	699.38	12.62	0.0093	
BC	591.68	1	591.68	10.67	0.0137	
A^2	1289.76	1	1289.76	23.27	0.0019	
B^2	1544.21	1	1544.21	27.86	0.0012	
C^2	1841.87	1	1841.87	33.23	0.0007	
Residual	388.04	7	55.43			
Lack of fit	371.22	5	74.24	8.82	0.1049	Not significant
Pure error	16.83	2	8.41			
Cor. total	14 357.31	16				

[a] Degree of freedom. [b] Evaluate the model's similarity to the residual (error) variance. [c] Chances of discovering the measured *F* value under the null hypothesis (significant at $p < 0.05$ and not significant at higher values).

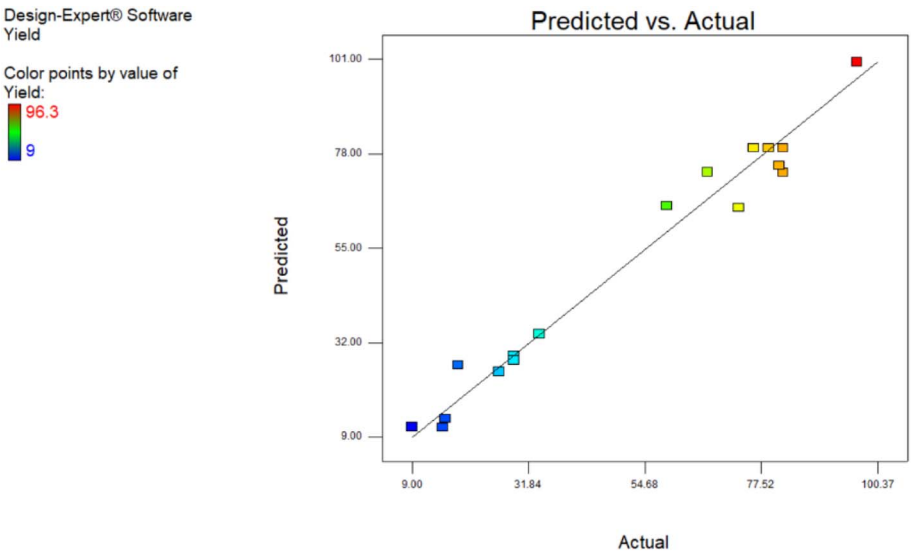

Fig. 5 Comparison of model data to experimental results.

Design-Expert software, the output of which can be seen in Table 2. The *F*-value is equal to 28, and the *P*-value for the presented model is around 0.0001. These values indicate the stability and validity of the model. Also, the value of R^2, which indicates the efficiency of the model, is equal to 11 003, and the value of R^2-adj, which indicates the degree of correlation between the experimental results and the predicted results, is equal to 13 008. These values show that the proposed model is very efficient in predicting the behavior of the system in the range of operating parameters used in the design.

As can be seen from the proposed model and the results of Table 2, among the parameters affecting the process, besides the specific effect of the reaction time and PTA percentage parameters with value-*F* values equal to 51 008 and 88 001, the catalyst amount (30 010) has a more prominent role. In order to predict the effects of the studied parameters on the value of oscillation, this software presented the following equations:

$$\text{Yield (\%)} = 79.47 + 14.40 \times \text{time} + 11.05 \times \text{catalyst loading} + 18.95 \times \text{PMA} - 6.28\text{time} \times \text{catalyst l} + 9.35\text{time} \times \text{PMA} + 8.60B \times \text{PMA} - 10.70 \times \text{time}^2 - 11.70 \times \text{catalyst loading}^2 - 12.78 \times \text{PMA}$$

The comparison between the predicted data from the software and the experimental data is shown in Fig. 5. This comparison shows that the proposed model has well predicted the study of mutual effects between factors and also their effects on the *C*-acylation process.

3.4.2 Possible mechanism. The possible reaction mechanism for the Friedel–Crafts *C*-acylation reaction over the catalysis of PMA@MIL-53 (Fe) is shown in Scheme 3. This process can be divided into two stages: activation of the electrophile and nucleophilic attack. The initial step is the coordination of the chlorine to the active sites of PMA@MIL-53 (Fe) which is then

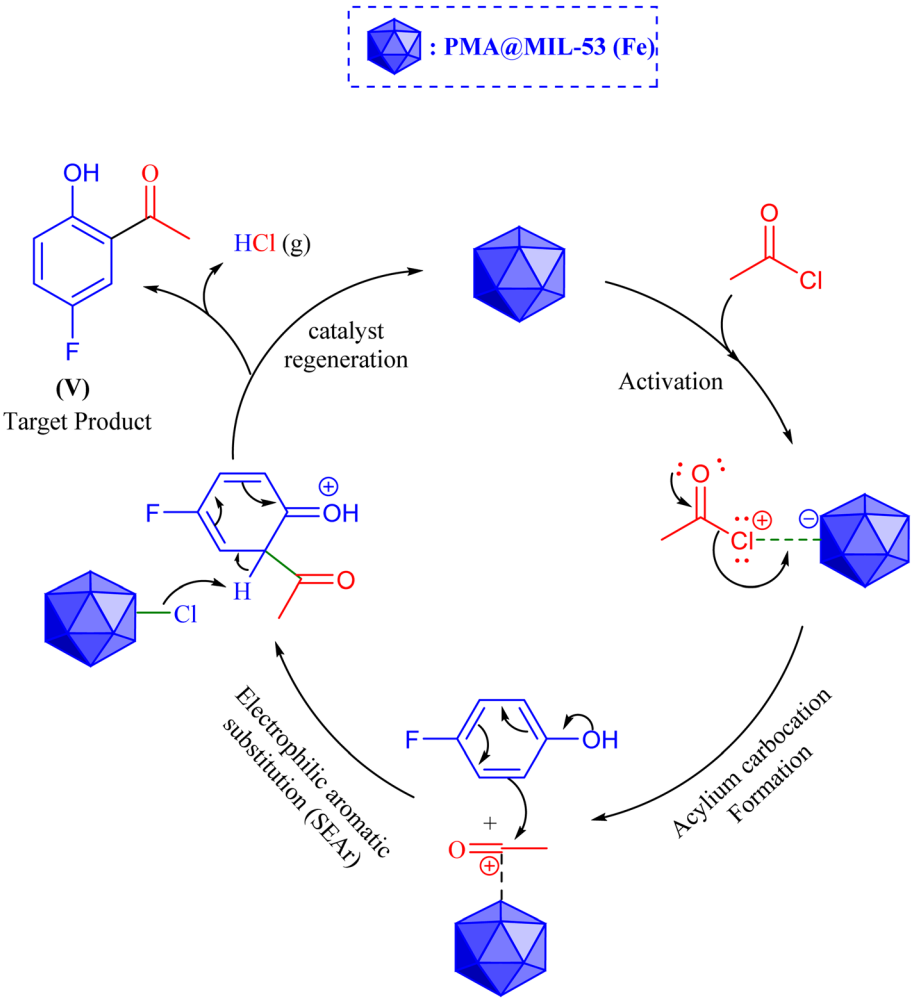

Scheme 3 Possible mechanism of the Friedel–Crafts *C*-acylation reaction over the catalysis of PMA@MIL-53 (Fe).

subjected to the elimination of an acylium carbocation followed by its complex formation with the acid catalyst. This complex is an electrophile that is highly reactive towards aromatic rings. The activated electrophile then undergoes electrophilic attack by the aromatic ring. The aromatic ring donates its electron density to the electrophile, which results in the formation of a new carbon–carbon bond. Finally, a proton is removed from the aromatic ring to restore its aromaticity and regenerate the catalyst.

3.4.3 Catalyst reusability. The use of heterogeneous catalysts in chemical processes is crucial for achieving sustainability and efficiency. One major advantage of these catalysts is their reusability, which helps to reduce reaction costs, minimize waste generation, and improve industrial process efficiency. To further investigate the potential of heterogeneous catalysts, the reusability of PMA@MIL-53 (Fe) was studied under optimal conditions. After each reaction, the catalyst was successfully filtered from the reaction mixture using a Büchner funnel and washed with ethyl acetate and acetone before being applied in subsequent runs. The results showed that the recycled catalyst could be reused up to five times without a significant decrease in its activity, as depicted in Fig. 6. This finding highlights the importance of developing sustainable and efficient chemical processes through the use of reusable catalysts like PMA@MIL-53 (Fe).

3.4.4 Hot filtration and leaching tests. Investigation was conducted to elucidate the nature of the PMA@MIL-53 (Fe) catalyst under optimal conditions, with a specific focus on potential PMA leaching and the structural stability of the catalyst. The hot filtration test revealed notable progress in the reaction by the halftime of reaction; however, progress ceased upon catalyst separation at this midpoint. Subsequent ICP analysis of the filtrate confirmed the absence of PMA. These findings strongly indicate that PMA remains securely bound to the MIL-53 (Fe) framework post-reaction, underscoring the catalyst's robust structural stability. This comprehensive understanding of the catalyst's heterogeneous nature highlights its potential for consistent and effective performance throughout multiple reuse cycles.

3.4.5 Comparison study of catalytic activity. In comparison to previously reported catalysts for the Friedel–Crafts *C*-acylation of *para*-fluorophenol, the PMA@MIL-53 (Fe) showed excellent performance (Table 3). For instance, the PMA@MIL-53 (Fe) catalyst had a shorter reaction time and a higher yield compared to previously reported catalysts. Furthermore, the catalyst exhibited

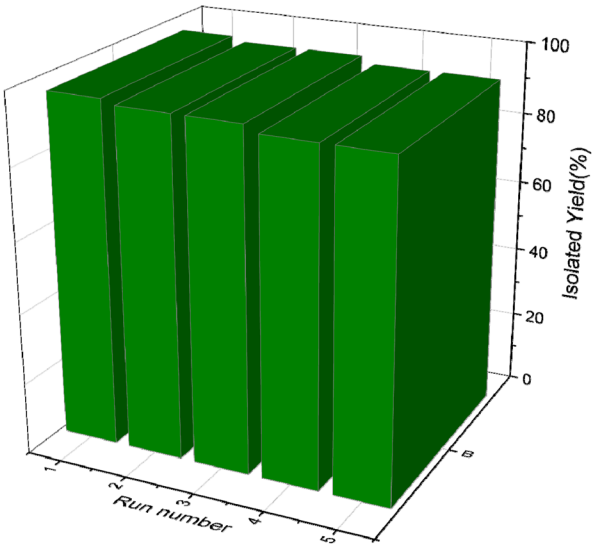

Fig. 6 Reusability of PMA@MIL-53 (Fe) in Friedel–Crafts *C*-acylation of *para*-fluorophenol.

Table 3 Comparison of the catalytic efficiency of PMA@MIL-53 (Fe) with those of other catalysts in model reactions

Entry	Catalyst	Time (min)	Yield (%)[a]	Reference
1	Aluminum chloride	120	89	29
2	Trifluoromethanesulfonic acid	180	93	30
3	PMA@MIL-53 (Fe)	42	96.3	This work

[a] Isolated yield.

high stability and reusability, retaining its activity after multiple runs. In addition, the methodology presented in this work is a green and efficient synthesis route, which makes it more environmentally friendly compared to other reported methods.

4. Conclusions

In this study, we utilized phosphomolybdic acid encapsulated in MIL-53 (Fe) as a heteropolyacid catalyst for the first time in the Friedel–Crafts acylation of *para*-fluorophenol. We investigated and optimized various parameters such as catalyst loading, PMA percentage, and reaction time using the response surface method. Our analysis showed that time and PMA percentage had the greatest effect on the production process. The optimal conditions for achieving the best efficiency were found to be 115 mg of catalyst containing 5.11 wt% of PMA for 30 minutes. Importantly, experiments on catalyst regeneration demonstrated its stability, and the yield of reactions did not vary considerably even after the catalyst was reused seven times.

Data availability

All data and materials in this publication are available by contacting the corresponding author.

Author Contributions

Reza Mehravar (the MSc student) performed most of the practical laboratory work as part of his master's thesis supervised by Dr Ahmad Nikseresht. Ahmad Nikseresht (supervisor, PhD) designed and coordinated the study, software, conceptualization, and edited the final version and submitted the manuscript for publication. Masoud Mohammadi (PhD) contributed to conceptualization, software, writing, review, and editing of the manuscript draft.

Conflicts of interest

The authors declare that they have no known competing financial interests or personal relationships that could have appeared to influence the work reported in this paper.

Acknowledgements

This work was financially supported by the Payame Noor University, Tehran, Iran.

References

1 M. A. Hadj and N. Masurier, Recent advances in aza Friedel-Crafts reaction: strategies for achiral and stereoselective synthesis, *Org. Chem. Front.*, 2023, **10**(7), 1847–1866, DOI: 10.1039/d2qo02018a.
2 T. Ahmad, S. Khan and N. Ullah, Recent Advances in the Catalytic Asymmetric Friedel-Crafts Reactions of Indoles, *ACS Omega*, 2022, **7**(40), 35446–35485, DOI: 10.1021/acsomega.2c05022.
3 R. B. Leveson-Gower and G. Roelfes, Biocatalytic Friedel-Crafts Reactions, *ChemCatChem*, 2022, **14**(18), e202200636, DOI: 10.1002/cctc.202200636.
4 N. Taheri, M. Dinari and M. Asgari, Recent Applications of Porous Organic Polymers Prepared via Friedel-Crafts Reaction under the Catalysis of AlCl3: A Review, *ACS Appl. Polym. Mater.*, 2022, **4**(9), 6288–6302, DOI: 10.1021/acsapm.2c00927.
5 A. Sumita and T. Ohwada, Friedel-Crafts-Type Acylation and Amidation Reactions in Strong Brønsted Acid: Taming Superelectrophiles, *Molecules*, 2022, **27**(18), 5984, DOI: 10.3390/molecules27185984.
6 V. Kumar, W. B. Turnbull and A. Kumar, Review on Recent Developments in Biocatalysts for Friedel–Crafts Reactions, *ACS Catal.*, 2022, **12**(17), 10742–10763, DOI: 10.1021/acscatal.2c01134.
7 M. Rachwalski, A. Buchcic-Szychowska and S. Leśniak, Recent advances in selected asymmetric reactions promoted by chiral catalysts: Cyclopropanations, friedel–crafts, mannich, michael and other zinc-mediated processes—an update, *Symmetry*, 2021, **13**(10), 1762, DOI: 10.3390/sym13101762.
8 D. Gaviña, M. Escolano, J. Torres, G. Alzuet-Piña, M. Sánchez-Roselló and C. del Pozo, Organocatalytic Enantioselective Friedel-Crafts Alkylation Reactions of Pyrroles, *Adv. Synth. Catal.*, 2021, **363**(14), 3439–3470, DOI: 10.1002/adsc.202100313.

9 K. K. Gangu and S. B. Jonnalagadda, A Review on Metal-Organic Frameworks as Congenial Heterogeneous Catalysts for Potential Organic Transformations, *Front. Chem.*, 2021, **9**, 747615, DOI: 10.3389/fchem.2021.747615.

10 Y. N. Nayak, S. Nayak, Y. F. Nadaf, N. S. Shetty and S. L. Gaonkar, Zeolite catalyzed friedel-crafts reactions: A review, *Lett. Org. Chem.*, 2020, **17**(7), 491–506, DOI: 10.2174/1570178616666190807101012.

11 A. Nikseresht, R. Bagherinia, M. Mohammadi and R. Mehravar, Phosphomolybdic acid hydrate encapsulated in MIL-53 (Fe): a novel heterogeneous heteropoly acid catalyst for ultrasound-assisted regioselective nitration of phenols, *RSC Adv.*, 2023, **13**(1), 674–687, DOI: 10.1039/D2RA07077D.

12 M. Koolivand, M. Nikoorazm, A. Ghorbani-Choghamarani and M. Mohammadi, A novel cubic Zn-citric acid-based MOF as a highly efficient and reusable catalyst for the synthesis of pyranopyrazoles and 5-substituted 1H-tetrazoles, *Appl. Organomet. Chem.*, 2022, **36**(6), 2641–2663, DOI: 10.1002/aoc.6656.

13 A. Ghorbani-Choghamarani, Z. Taherinia and M. Mohammadi, Facile synthesis of Fe3O4@GlcA@Ni-MOF composites as environmentally green catalyst in organic reactions, *Environ. Technol. Innovation*, 2021, **24**, 102050, DOI: 10.1016/j.eti.2021.102050.

14 N. Hussain-Khil, A. Ghorbani-Choghamarani and M. Mohammadi, A new silver coordination polymer based on 4,6-diamino-2-pyrimidinethiol: synthesis, characterization and catalytic application in asymmetric Hantzsch synthesis of polyhydroquinolines, *Sci. Rep.*, 2021, **11**(1), 15657, DOI: 10.1038/s41598-021-94846-6.

15 C. Li, H. Lv, K. Yang and X. Zhang, Robust Fluorine-Functionalized {Ln5}-Organic Frameworks for Excellent Catalytic Performance on Cycloaddition of CO2 with Epoxides and Knoevenagel Condensation, *ACS Appl. Mater. Interfaces*, 2023, **15**(29), 35052–35061, DOI: 10.1021/acsami.3c06804.

16 B. Zhao, C. Li, T. Hu and X. Zhang, Nanoporous {Pb3}-Organic Framework for Catalytic Cycloaddition of CO2 with Epoxides and Knoevenagel Condensation, *ACS Appl. Nano Mater.*, 2023, **6**(24), 23196–23206, DOI: 10.1021/acsanm.3c04586.

17 H. Keypour, J. Kouhdareh, S. Alavinia, K. Rabiei, M. Mohammadi, A. Maryamabadi, *et al.*, Post-synthetic modification of dual-porous UMCM-1-NH2 with palladacycle complex as an effective heterogeneous catalyst in Suzuki and Heck coupling reactions, *J. Organomet. Chem.*, 2023, **989**, 122646, DOI: 10.1016/j.jorganchem.2023.122646.

18 F. Ghobakhloo, D. Azarifar, M. Mohammadi, H. Keypour and H. Zeynali, Copper(II) Schiff-Base Complex Modified UiO-66-NH2(Zr) Metal-Organic Framework Catalysts for Knoevenagel Condensation-Michael Addition-Cyclization Reactions, *Inorg. Chem.*, 2022, **61**(12), 4825–4841, DOI: 10.1021/acs.inorgchem.1c03284.

19 J. Yin, W. Li, W. Li, L. Liu, D. Zhao, X. Liu, *et al.*, Heterometallic ZnHoMOF as a dual-responsive luminescence sensor for efficient detection of hippuric acid biomarker and nitrofuran antibiotics, *Molecules*, 2023, **28**(17), 6274, DOI: 10.3390/molecules28176274.

20 F. Wang, D. Zhao, W. Li, H. Zhang, B. Li, T. Hu, *et al.*, Rod-shaped units based cobalt(II) organic framework as an efficient electrochemical sensor for uric acid detection in serum, *Microchem. J.*, 2023, **185**, 108154, DOI: 10.1016/j.microc.2022.108154.

21 A. M. Naseri, M. Zarei, S. Alizadeh, S. Babaee, M. A. Zolfigol, D. Nematollahi, *et al.*, Synthesis and application of [Zr-UiO-66-PDC-SO3H]Cl MOFs to the preparation of dicyanomethylene pyridines via chemical and electrochemical methods, *Sci. Rep.*, 2021, **11**(1), 16817, DOI: 10.1038/s41598-021-96001-7.

22 A. Nikseresht, A. Daniyali, M. Ali-Mohammadi, A. Afzalinia and A. Mirzaie, Ultrasound-assisted biodiesel production by a novel composite of Fe(III)-based MOF and phosphotangestic acid as efficient and reusable catalyst, *Ultrason. Sonochem.*, 2017, **37**, 203–207, DOI: 10.1016/j.ultsonch.2017.01.011.

23 A. K. Dizaji, B. Mokhtarani and H. R. Mortaheb, Deep and fast oxidative desulfurization of fuels using graphene oxide-based phosphotungstic acid catalysts, *Fuel*, 2019, **236**, 717–729, DOI: 10.1016/j.fuel.2018.09.076.

24 C. Peinado, J. M. Campos-Martin and S. Rojas, Phosphotungstic acid catalysed bioethylene synthesis under industrially relevant conditions, *React. Chem. Eng.*, 2023, **8**(4), 815–823, DOI: 10.1039/D2RE00354F.

25 H. Zhu and R. Wang, Phosphotungstic acid-promoted Mn-Fe bimetal oxide with high sulfur resistance for low-temperature selective catalytic reduction of nitrogen oxides with NH3, *J. Alloys Compd.*, 2023, **936**, 168272, DOI: 10.1016/j.jallcom.2022.168272.

26 Z. Liu, X. Peng, Y. Xu, T. Tang, S. Wei, B. Liu, *et al.*, Macromolecular structural characteristics and functional potential of tobacco stalk lignin from the phosphotungstic acid-assisted delignification process, *Biomass Bioenergy*, 2023, **170**, 106706, DOI: 10.1016/j.biombioe.2023.106706.

27 H. Luo, Y. Gu, D. Liu and Y. Sun, Advances in oxidative desulfurization of fuel oils over mofs-based heterogeneous catalysts, *Catalysts*, 2021, **11**(12), 1557, DOI: 10.3390/catal11121557.

28 S. Parak, A. Nikseresht, M. Alikarami and S. Ghasemi, RSM optimization of biodiesel production by a novel composite of Fe(III)-based MOF and phosphomolybdic acid, *Res. Chem. Intermed.*, 2022, **48**(9), 3773–3793, DOI: 10.1007/s11164-022-04783-w.

29 N. X. Wang, A. G. Yu, G. X. Wang, X. H. Zhang, Q. S. Li and Z. Li, Synthesis of (S , R , R , R)-α,α′-Iminobis(methylene) bis(6-fluoro-3 H ,4 H -dihydro-2 H -1-benzopyran-2-methanol), *Synthesis*, 2007, **2007**(8), 1154–1158, DOI: 10.1055/s-2007-965993.

30 R. Murashige, Y. Hayashi, S. Ohmori, A. Torii, Y. Aizu, Y. Muto, *et al.*, Comparisons of O-acylation and Friedel–Crafts acylation of phenols and acyl chlorides and Fries rearrangement of phenyl esters in trifluoromethanesulfonic acid: effective synthesis of optically active homotyrosines, *Tetrahedron*, 2011, **67**(3), 641–649, DOI: 10.1016/j.tet.2010.11.047.